Proceedings of the ASME-JSME-KSME 2011 Joint Fluids Engineering Conference
AJK-Fluids2011
July 24-29, 2011, Hamamatsu, Shizuoka, JAPAN

AJK2011-36005

AN ESTIMATION OF THERMODYNAMIC AND TRANSPORT PROPERTIES OF CRYOGENIC HYDROGEN USING CLASSICAL MOLECULAR SIMULATION

Hiroki Nagashima
Tohoku University
Sendai, Miyagi, Japan

Takashi Tokumasu
Tohoku University
Sendai, Miyagi, Japan

Shin-ichi Tsuda
Shinshu University
Nagano, Nagano, Japan

Nobuyuki Tsuboi
Kyushu Institute of Technology
Kitakyushu, Fukuoka, Japan

Mitsuo Koshi
University of Tokyo
Bunkyo, Tokyo, Japan

A. Koichi Hayashi
Aoyama Gakuin University
Sagamihara, Kanagawa, Japan

ABSTRACT

In this paper, we estimated the thermodynamic and transport properties of cryogenic hydrogen using classical molecular simulation to clarify the limit of classical method on the estimation of those properties of cryogenic hydrogen. Three empirical potentials, the Lennard-Jones (LJ) potential, two-center Lennard-Jones (2CLJ) potential, and modified Buckingham (exp-6) potential, and an *ab initio* potential model derived by the molecular orbital (MO) calculation were applied. Molecular dynamics (MD) simulations were performed across a wide density-temperature range. Using these data, the equation of state (EOS) was obtained by Kataoka's method, and these were compared with NIST (National Institute of Standards and Technology) data according to the principle of corresponding states. Moreover, we investigated transport coefficients (viscosity coefficient, diffusion coefficient and thermal conductivity) using time correlation function. As a result, it was confirmed that the potential model has a large effect on the estimated thermodynamic and transport properties of cryogenic hydrogen. On the other hand, from the viewpoint of the principle of corresponding states, we obtained the same results from the empirical potential models as from the *ab initio* potential, showing that the potential model has only a small effect on the reduced EOS: the classical MD results could not reproduce the NIST data in the high-density region. This difference is thought to arise from the quantum effect in actual liquid hydrogen.

INTRODUCTION

Currently liquid hydrogen is used as fuel for fuel cells and propellant for liquid rocket engines and the demand for liquid hydrogen is increasing. Therefore, it is very important to accurately ascertain the thermal flow phenomena which occur in the liquid hydrogen for safety and efficient use. Especially, in the case of analysis of nanoscale phenomena, molecular simulation is a powerful method. In recent years, studies that clarify the thermodynamic and transport properties of liquid hydrogen using molecular simulation [1-4] have attracted attention. It is possible to calculate macroscopic thermodynamic properties from the microscopic information using an intermolecular interaction. However there is a problem in the molecular simulation of liquid hydrogen. It is how to treat low-temperature quantum effect. The rotational characteristic temperature of hydrogen is higher than those of other liquids, and the thermal de Broglie wavelength is on the same order as the molecular diameter of hydrogen. Therefore, it is not possible to simply apply the classical method to simulations of liquid hydrogen.

Clearly, the non-classical approach for approximating quantum effects should be applied for such a system. It is especially desired in physics and chemistry to reproduce the time evolution of quantum many-body system, such as liquid hydrogen. Accordingly many studies of such simulations have been conducted and new methods have been proposed [5-16]. Among these, path integral centroid molecular dynamics (PICMD) [5-9], proposed by Cao and Voth is a useful method. At present, however, these simulations are performed with few simulation conditions for estimation of thermodynamics and transport properties [1-4], because the calculation loads using

these methods are large. From this reason, the non-classical methods are difficult to apply for analysis of thermal flow phenomena in molecular level. Moreover, fundamentally the simulation must be conducted across a wide temperature-density range to accurately estimate the thermodynamic properties of liquid hydrogen. From this viewpoint, it is very difficult to perform such simulations using non-classical method. In general, the classical method is suitable for large calculations because of the required calculation load. However accurate analysis of thermodynamics and transport properties of cryogenic hydrogen using classical method has not been studied. Therefore the effect of intermolecular interaction models on the estimated thermodynamic and transport properties of cryogenic hydrogen and the influence of quantum effects on the equation of state have not been clarified. Therefore, the limits of classical simulation methods on the analysis of thermodynamic and transport properties of cryogenic hydrogen have not been defined.

For this reason, the purpose of this study is clearly determining the limits of classical molecular simulation method on the estimation of cryogenic hydrogen. Specifically, EOSs of cryogenic hydrogen were derived from simulation across a wide temperature-density range using four intermolecular potential models and diffusion coefficient, viscosity coefficient and thermal conductivity were calculated using Green-Kubo method. The effect of intermolecular interaction models on the estimated thermodynamic and transport properties of cryogenic hydrogen is clarified by comparing empirical potentials used for conventional classical simulation with an *ab initio* potential derived by molecular orbital (MO) calculation. In addition, the differences between EOSs, transport coefficients and experimental results are investigated using the principle of corresponding states.

INTERMOLECULAR POTENTIAL MODEL

Empirical Potential Models

The Lennard-Jones (LJ) potential, two-center Lennard-Jones (2CLJ) potential [17] and modified Buckingham (exp-6) potential [18] described below were used to express the intermolecular interactions. The LJ potential is a standard potential that has been used in many molecular simulations. As shown in Fig. 1, the 2CLJ potential can express the shape of diatomic molecules by internuclear distance. The exp-6 potential allows the slope of the exponential repulsion to be changed. The shape of these potentials are expressed by

$$\varphi_{\mathrm{LJ}}(r)=4\varepsilon\left\{\left(\frac{\sigma}{r}\right)^{12}-\left(\frac{\sigma}{r}\right)^{6}\right\}, \tag{1}$$

$$\varphi_{2\mathrm{CLJ}}(r)=\sum_{a=1}^{2}\sum_{b=1}^{2}\varphi_{\mathrm{LJ}}\left(r_{iajb}\right), \tag{2}$$

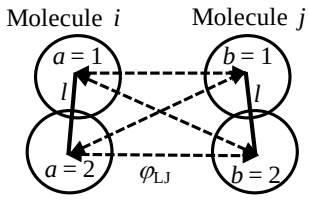

FIGURE 1. 2CLJ POTENTIAL MODEL.

$$\varphi_{\exp-6}(r)=\begin{cases}\dfrac{\varepsilon}{1-6/d}\left[\dfrac{6}{d}\exp\left\{d\left(1-\dfrac{r}{r_{\min}}\right)\right\}-\left(\dfrac{r_{\min}}{r}\right)^{6}\right] & r\geq r_{\max}\\ \infty \quad r\leq r_{\max}\end{cases}, \tag{3}$$

where σ and ε are the potential parameters corresponding to the molecular diameter and the depth of the potential well, respectively. In Eq. (2), a and b denote nuclei belonging to molecules i and j, respectively, and r_{iajb} denotes the distance between nucleus a of molecule i and nucleus b of molecule j. In addition, the 2CLJ potential has an additional parameter, the internuclear distance l. This potential is able to express the molecular rotational motion using l. The molecular size is bigger and the moment of inertia is larger with the increase in l. In Eq. (3), $r_{\min}$ is the value of r for the energy minimum, d denotes the steepness of the exponential repulsion, with high d corresponding to steeper potential and $r_{\max}$ is the value of the minimum r for which $\varphi_{\exp\text{-}6}(r)$ has a spurious maximum r_{max}. The ratio $r_{\max}/r_{\min}$ is given by the smallest root of the equation

$$\left(\frac{r_{\max}}{r_{\min}}\right)^{7}\exp\left\{d\left(1-\frac{r_{\max}}{r_{\min}}\right)\right\}=1. \tag{4}$$

Ab Initio Potential Model

The *ab initio* potential [19] was derived by MO calculation. GAUSSIAN03 was used for this calculation, in which the combination of electronic correlation function and basis set to solve the Schrödinger equation was chosen to CCSD(T)/aug-cc-PVQZ. The coordinates of this potential model are shown in Fig. 2 and the potential function is described by Eq. (5). In this study, the potential function was expressed by spherical harmonics. Moreover, in the case of homonuclear diatomic molecules, odd quantum numbers do not appear, and therefore

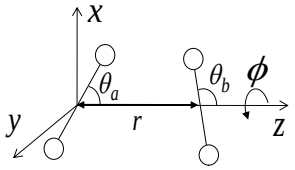

FIGURE 2. COORDINATE OF THE *AB INITIO* POTENTAIL FUNCTION MODEL.

this function is expressed by five even quantum number potential modes φ^{000}, φ^{202} (φ^{022}), φ^{220}, φ^{222}, φ^{224}. The potential modes are expressed by Eq. (6),

$$\begin{aligned}\varphi_{ab}(r,\theta_i,\theta_j,\phi) &= \varphi^{000} + \sqrt{5}[\varphi^{202}P_2^0(\cos\theta_a) + \varphi^{022}P_2^0(\cos\theta_b)] \\ &+ \frac{\sqrt{5}}{12}\left[\varphi^{220} + 2\sqrt{\frac{5}{14}}\varphi^{222} + \sqrt{\frac{1}{14}}\varphi^{224}\right]P_2^2(\cos\theta_a)P_2^2(\cos\theta_b)\cos 2\phi \\ &+ \frac{\sqrt{5}}{3}\left[\varphi^{220} - \sqrt{\frac{5}{14}}\varphi^{222} - 4\sqrt{\frac{1}{14}}\varphi^{224}\right]P_2^1(\cos\theta_a)P_2^1(\cos\theta_b)\cos\phi \\ &+ \sqrt{5}\left[\varphi^{220} - 2\sqrt{\frac{5}{14}}\varphi^{222} + 6\sqrt{\frac{1}{14}}\varphi^{224}\right]P_2^0(\cos\theta_a)P_2^0(\cos\theta_b)\end{aligned} \quad ,(5)$$

$$\varphi^{l_a l_a l}(r) = C_1\exp\left(-C_2 r - C_3 r^2\right) - C_4 r^{-6} - C_5 r^{-8} - C_6 r^{-10}, \quad (6)$$

where the unit of r is Å and $P_2(\cos\theta)$ are the associated Legendre polynomials and the coefficients (C_1 to C_6) were determined for each quantum number potential mode by fitting the MO results. The coefficient for each potential mode are shown in Tab. 1.

TABLE.1 THE COEFFICIENTS OF EACH MODE OF *AB INITIO* POTENIAL MODEL.

	φ^{000}	φ^{202} (φ^{022})	φ^{220}	φ^{222}	φ^{224}
P_1	3035.3	19.937	0.015380	0.0000	0.0000
P_2	2.4251	0.74047	6.6452	326.36	0.0000
P_3	0.22082	0.53027	0.46822	15.620	0.0000
P_4	202.71	16.875	-1.3162	1.0672	-20.721
P_5	-81.244	-67.597	15.170	-8.3913	-10.196
P_6	-110.28	6.7525	-1.6478	8.1694	-30.744

SIMULATION METHOD

Calculation Method of EOS

The EOS was determined by Kataoka's method [20]. In this method, the EOS is expressed by the excess Helmholtz free energy from an ideal gas A^e as the sum of the product of density ρ and temperature T,

$$\frac{\beta A^e}{N} = \sum_{n=1}^{5}\sum_{m=-1}^{5} A_{mn}\left(\frac{\rho}{\rho_0}\right)^n\left(\frac{\beta}{\beta_0}\right)^m, \quad (7)$$

where $\beta = 1/(k_B T)$, and N is the number of molecules. The coefficients, ρ_0 and β_0, were introduced in order to make the coefficient in Eq. (7), A_{mn}, dimensionless and were set at $\rho_0 = m/\sigma^3$ and $\beta_0 = 1/\varepsilon$, respectively. The internal energy E_p and pressure p are obtained using A^e by

$$\frac{\beta E_p}{N} = \beta\left\{\frac{\partial}{\partial\beta}\left(\frac{\beta A^e}{N}\right)\right\}_\rho, \quad (8)$$

$$\frac{\beta p}{\rho} - 1 = \rho\left\{\frac{\partial}{\partial\rho}\left(\frac{\beta A^e}{N}\right)\right\}_\beta, \quad (9)$$

respectively. In this study, the internal energy and pressure could be obtained by microcanonical ensemble MD simulation [20]. The three empirical potential models and the *ab initio* potential were applied to this MD calculation. The 35 A_{mn} coefficients in Eq. (7) were derived by a least square fitting of the simulated potential energies and pressures. Details of the method are described below.

The cubic cell used in the simulations contained 2048 molecules. The length of the cell was set at $L = (N/\rho)^{1/3}$, where ρ is number density. Periodic boundary conditions were applied in all direction. For the initial conditions, the molecules were placed in an fcc lattice structure and $\boldsymbol{\upsilon}_i$, the velocity vector of molecule i, was given according to the Boltzmann distribution at temperature T. Time integration of the equation of motion was performed using the velocity Verlet algorithm [21-23]. The dimensionless time step reduced by $\sigma\sqrt{m/\varepsilon}$ was set at $\Delta t^* = 0.0025$. In the case of the exp-6 potential, $r_{\min}$ was used to reduce the time step instead of σ, and the time step was set at $\Delta t^* = 0.0045$. In the case of the *ab initio* potential, Δt was set at 1fs and $m = 2.016 \times 10^{-3}/N_A$ kg, where N_A is Avogadro's number. In the case of the empirical potential models, the cutoff distance for the intermolecular force was $r_c^* = 5$, while $r_c = 18$ Å in the case of the *ab initio* potential. The MD simulations were performed controlling the temperature of the system by velocity scaling during the initial 2000 steps to establish an equilibrium state at temperature T and without controlling the temperature during the next 18000 steps. Sample data were taken only from the later 18000 steps. The temperature T, pressure P, and excess internal energy, E_p were determined by

$$T = \frac{2}{3Nk_B}\sum_{i=1}^{N}\left\langle\frac{1}{2}m\upsilon_i^2\right\rangle, \quad (10)$$

$$P = \frac{Nk_B\langle T\rangle}{V} + \frac{1}{3V}\left\langle\sum_{i=1}^{N}\sum_{j>i}^{N}\boldsymbol{r}_{ij}\cdot\boldsymbol{F}_{ij}\right\rangle + \Delta P, \quad (11)$$

$$E_p = \left\langle\sum_{i=1}^{N}\sum_{j>i}^{N}\varphi(r)\right\rangle + \Delta E_p, \quad (12)$$

respectively, where N denotes the number of molecules, V denotes the volume of the system, and $\boldsymbol{r}_{ij}$ denotes the vector from the center of mass of molecule j to that of molecule i. Vector $\boldsymbol{F}_{ij}$ is the force from molecule j to molecule i. The brackets < > represent the long time average. In the case of the *ab initio* potential, pressure was calculated using the virial

theorem. However the force contributing to the virial term is not the total force acting on a molecule but only the part of the force that acts by displacement of $\boldsymbol{r}_{ij}$, as described below

$$P = \frac{Nk_BT}{V} + \frac{1}{3V}\left\langle \sum_{i=1}^{N}\sum_{j>i}^{N} \frac{\partial \varphi_{ij}}{\partial \boldsymbol{r}_{ij}} \boldsymbol{r}_{ij} \right\rangle + \Delta P \,, \tag{13}$$

where ΔP is the long-ranged intermolecular interaction correction of pressure and ΔE_p is the internal energy. These were calculated from the following expressions

$$\Delta P = -\frac{N\rho}{6V}\int_{r_c}^{\infty} r \frac{d\varphi(r)}{dr} g(r) 4\pi r^2 dr \,, \tag{14}$$

$$\Delta E_p = \frac{\rho}{2}\int_{r_c}^{\infty} \varphi(r)\, g(r) 4\pi r^2 dr \,, \tag{15}$$

where $g(r)$ is a distribution function, which was assumed to be 1.

In the case of the 2CLJ and *ab initio* potentials, molecular rotational motion was described in the molecular coordinate system. In this system, the position of the two nuclei of a molecule were (0, 0, l/2) and (0, 0, -l/2), respectively. In the case of the *ab initio* potential, l was set at 0.74 Å. The rotational energy of molecule i, e_{ri}, was given by the Boltzmann distribution at temperature T, and the angular velocity vector of molecule i was $\omega_i = \left(\sqrt{2e_{ri}/I}, 0, 0\right)$ in the molecular coordinate system, where $I = 0.25ml^2$ denotes the moment of inertia of the molecule. The orientation of the molecule was described by the Euler angle (θ, ϕ, ψ) [21]. The initial Euler angles were set at $\phi_i = 2\pi R$, $\theta_i = \cos^{-1}R$, and $\psi_i = 2\pi R$, respectively, where $0 < R < 1$ and R was random number and was given the uniform distribution. The molecular rotational motion was calculated using quaternion [21]. When considering molecular rotational motion, the temperature T, was determined by

$$T = \frac{2}{5Nk_B}\sum_{i=1}^{N}\left\langle \frac{1}{2}mv_i^2 + \frac{1}{2}\omega_i \cdot \boldsymbol{I} \cdot \omega_i \right\rangle. \tag{16}$$

In this study, calculations were performed using the following dimensionless density-temperature simulation conditions,

$$\rho^* = \frac{\rho\sigma^3}{m} \,, \tag{17}$$

$$T^* = \frac{k_BT}{\varepsilon} \,, \tag{18}$$

$$P^* = \frac{P\sigma^3}{\varepsilon} \,. \tag{19}$$

In the case of the exp-6 potential, $r_{\min}$ was used in place of σ in Equation (17)-(19). The first 160 state points were defined by selecting twenty values of ρ^* (0.001, 0.01, 0.05, 0.1, 0.15, 0.2, 0.25, 0.3, 0.35, 0.4, 0.45, 0.5, 0.55, 0.6, 0.65, 0.7, 0.75, 0.8, 0.85, 0.9) and eight values of T^*(1.5, 2.0, 2.5, 3.0, 3.5, 4.0, 4.5, 5.0). Pressure and internal energy were calculated at each point. However, these points did not necessarily cover the temperature and density ranges necessary for determining the EOS. Therefore, new state points were selected in the nondimensional space of densities and temperatures which were reduced by the critical density, temperature and pressure derived by Kataoka's method. The reduced values are expressed by the following equations,

$$\rho' = \frac{\rho^*}{\rho^*_{\mathrm{cr}}} \,, \tag{20}$$

$$T' = \frac{T^*}{T^*_{\mathrm{cr}}} \,, \tag{21}$$

$$P' = \frac{P^*}{(\rho^*_{\mathrm{cr}} k_B T^*_{\mathrm{cr}}/m)} \,. \tag{22}$$

A second set of 304 state points were defined by selecting sixteen values of ρ' (0.01, 0.05, 0.1, 0.15, 0.2, 0.3, 1.9, 2.0, 2.1, 2.2, 2.3, 2.4, 2.5, 2.6, 2.8, 3.0) and nineteen value of T' (0.4, 0.45, 0.5, 0.55, 0.6, 0.65, 0.7, 0.75, 0.8, 0.85, 0.9, 0.95, 1.0, 1.05, 1.1, 1.15, 1.2, 1.25, 1.3). In the case of the empirical potential, MD simulations were performed using nondimensional simulation conditions, in order to clarify the effect of potential parameter l/σ and d. In contrast, in the case of the *ab initio* potential, MD simulations were performed using dimensional simulation conditions, because each potential parameter was strictly defined in the MO calculation. The temperature simulation condition range was 14 to 50 K, density condition range was 0.01 to 105 kg/m^3, number of total condition was 302 states.

These selected points, however, included those at which the system was in two phases. If the system is in two phases, the internal energies and pressures cannot be calculated exactly. And thus, it is necessary to exclude such state points from those used to calculate the EOS. In particular, it has been reported that in MD simulations the temperature of a system deviates greatly when the system is in the two-phase state [24]. Therefore the data points for which the averaged (mean) temperature over the sampled steps deviated by more than 5% from the target temperature were regarded as two-phase cases and were excluded from the data set used to determine the EOS. In the case of the *ab initio* potential, however, this method to determine the two-phase condition was found to be ineffective. Accordingly, the two-phase system was recognized by the number of *voids*. In this method, the cubic cell was divided into very small volumes and whether any molecule existed within a radius of c of each grid point was checked using the molecular position at the end of the simulation. The points where no molecule existed within a radius of c were regarded as void, and the total number of void was called *void number*. The radius c was set at c=L/10, to fit the small volume cell size. The cell

length was chosen such that it was longer than the initial intermolecular distance and was able to confirm the change of void number. It was confirmed that in the case of $c=L/10$, the void number increases rapidly to 60 when a system is in two phases. In this study, therefore, the data for which the void number is more than 60 were regarded as two-phase cases, and were excluded from those used to obtain the EOS.

It is probable that a system is in a solid state in high-density and low temperature regions. In this study, the data for which the mean square displacement during the simulation is less than 5σ were regarded as solid state cases and were excluded from those used to obtain the EOS. Moreover, the data inside the spinodal line were also excluded, because these data were considered to correspond to two-phase states. The EOS was calculated using the remaining data. The spinodal line obtained from the new EOS might differ from the previous one, and so this calculation must be performed iteratively.

The EOS was repeatedly calculated until the spinodal line converged. The EOS at T=20 K (T/T^*_{cr}=0.603) using LJ potential is shown in Fig. 3, which shows that the EOS obtained in this study agreed well with the MD results. Consequently, this EOS is able to reproduce the state of the system.

The spinodal line was obtained using this EOS. This method is described as follows. The spinodal line was an envelope determined by the points where

$$\left(\frac{\partial P}{\partial \rho}\right)_T = 0 \tag{23}$$

was satisfied. A saturation line was also obtained using the EOS and the following two relations,

$$P_{gas} = P_{liq}, \quad G_{gas} = G_{liq}, \tag{24}$$

where G is Gibbs free energy described by the equation

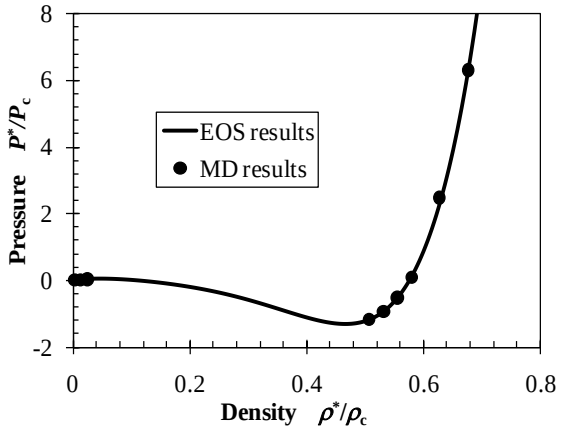

FIGURE 3. COMPARISION OF MD SIMULATION RESULTS OF LJ POTENIAL MODEL AND EOS WHICH DERIVED BY KATAOKA'S METHOD AT T = 20 K (T/T^*_{cr} = 0.6034).

$$G = A^e + A_0 + PV, \tag{25}$$

in which A_0 is Helmholtz free energy at the dilute limit and is obtained from $A_0 \approx -Nk_BT\ln(V/\Lambda^3 N)$, in which Λ is the thermal de Broglie wavelength. In the case of calculating saturation, it is not necessary to consider the part of A_0 that depends only on temperature because only the change of Gibbs free energy on the isothermal line should be considered. Therefore the temperature term of A_0 is ignored and Gibbs free energy is described by

$$G = A^e + Nk_BT\ln\rho + PV \tag{26}$$

The Gibbs free energies in liquid and vapor phase were obtained using Eq. (26), and saturation density in the liquid and vapor phases, ρ_v and ρ_l, respectively, were obtained as the combination of densities that satisfies Eq. (24). In this method, however, the accuracy of the saturation line near the critical point is insufficient and therefore the critical temperature, density, and pressure were calculated accurately using the following relations [25]

$$\frac{1}{2}(\rho_l + \rho_v) = AT + B, \tag{27}$$

$$\rho_l - \rho_v = C\left(1 - \frac{T}{T_{cr}}\right), \tag{28}$$

where A, B and C are constants. The calculation results of the critical temperature T^*_{cr}, density ρ^*_{cr}, pressure P^*_{cr}, spinodal line, and saturation line with LJ potential are shown in Tab. 2 and Fig. 4. The critical temperature T_{cr}, density ρ_{cr}, pressure P_{cr}, spinodal line, and saturation line with *ab initio* potential are shown in Tab. 3 and Fig. 5. Where ● represents rejected

TABLE. 2 THE CRITICAL TEMPERATURE, DENSITY AND PRESSURE OF THE FLUID WITH EACH EMPIRICAL POTENAL.

Potential model	T^*_{cr}	ρ^*_{cr}	P^*_{cr}
LJ	1.333	0.3262	0.1480
2CLJ (l/σ = 0.2)	4.378	0.2867	0.4235
2CLJ (l/σ = 0.4)	3.185	0.2428	0.2504
2CLJ (l/σ = 0.6)	2.475	0.2005	0.1636
2CLJ (l/σ = 0.8)	2.063	0.1783	0.1233
2CLJ (/σ = 1.0)	1.797	0.1533	0.0901
exp-6 (d=10)	2.043	0.3935	0.3280
exp-6 (d=20)	1.116	0.3203	0.1399
exp-6 (d=30)	0.975	0.3230	0.1114

TABLE. 3 THE CRITICAL TEMPERATURE, DENSITY AND PRESSURE OF THE FLUID WITH *AB INITIO*POTENAL.

	T_{cr} [K]	ρ_{cr} [kg/m^3]	P_{cr} [MPa]
NIST	33.145	31.263	1.2964
ab-initio potential	45.502	38.753	2.4889

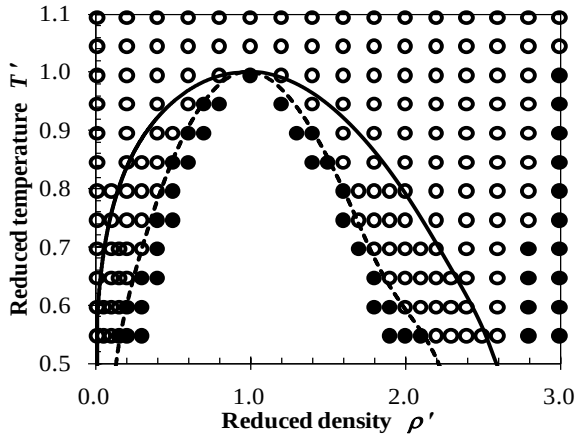

FIGURE 4. RELATIONSHIP BETWEEN SATURATION LINE, SPINODAL LINE AND DIMULATED POINTS USING LJ PPOTENTIAL. SLOID LINE DENOTES SATURATION LINE, DASH LINE DENOTES SPINODAL LINE, ● DENOTES REJECTED POINTS.

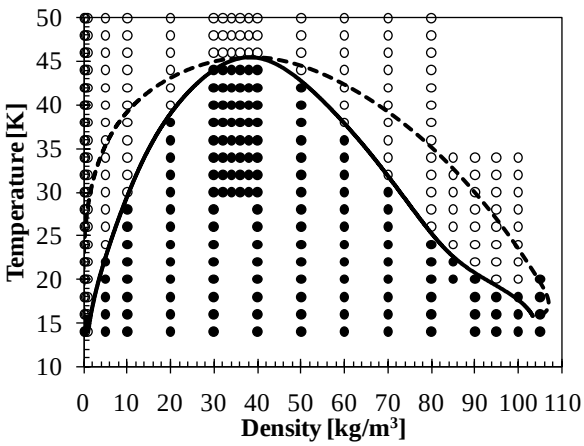

FIGURE 5. RELATIONSHIP BETWEEN SATURATION LINE, SPINODAL LINE AND SIMULATED POINTS USING *AB INITIO* POTENTIAL. SLOID LINE DENOTES SATURATION LINE, DASH LINE DENOTES SPINODAL LINE, ● DENOTES REJECTED POINTS.

points when determining the EOS. As shown in Fig. 5, in the MD results using the *ab initio* potential, the system was in a two-phase state or solid state in the high-density and low-temperature (less than 20 K) regions.

In the case of the 2CLJ and exp-6 potentials, all physical quantities were function of l/σ and d when σ ($r_{\min}$) and ε were used for dimensionless expression. The dependence of these potentials on hydrogen properties were analyzed by changing l/σ and d. Simulations were performed at l/σ = 0.2, 0.4, 0.6, 0.8, and 1.0 and d = 10, 20, and 30. Moreover, each thermodynamic property was reduced by each critical point in order to analyze qualitative agreement with the NIST data using the principle of corresponding state.

Calculation Method of Transport Coefficients

In this paper, self-diffusion coefficient as one of transport coefficients was calculated using Green-Kubo method. In this method, transport coefficients are expressed by integration of correlation function. Transport coefficient is obtained by

$$K = \int_0^\infty \left\langle \dot{A}(t) \cdot \dot{A}(0) \right\rangle dt \,, \tag{29}$$

where K is transport coefficient, $\dot{A}(t)$ is the flux of physical quantity $A(t)$, < > represents the ensemble average. Right hand side term is called time correlation function. In the case of self-diffusion coefficient D_S, $K = 3D_S$, and

$$\dot{A}(t) = \boldsymbol{\upsilon}_i(t) \,, \tag{30}$$

where $\boldsymbol{\upsilon}_i$ is velocity of molecule.

In this paper, self-diffusion coefficient was calculated near the triple point of LJ liquid. The triple point of LJ liquid is T^*/T_{cr}^* = 0.6079, ρ^*/ρ_{cr}^* = 2.640[31]. In the case of calculation of transport coefficients, long computational time is necessary for accurate analysis. Therefore, the number of time steps was set to 1 million steps.

COMPARSION OF SATURATION LINE

The temperature-density saturation line and temperature-pressure saturation line which were reduced by critical temperature T^*_{cr}, critical density ρ^*_{cr}, and critical pressure P^*_{cr} are shown in Fig. 6 and Fig. 7. In this figure, the NIST data also has been reduced by the critical point of hydrogen (critical temperature 33.145 K, critical density 31.263 kg/m^3, and critical pressure 1.263 MPa) [26]. As shown in Fig. 6, empirical potentials which were used in this study do not reproduce the thermodynamic properties of cryogenic hydrogen in the whole temperature region below the critical temperature. In the case of 2CLJ potential, saturation pressure of each potential model was underestimated relative to NIST data in the whole temperature region below the critical temperature. From these results, the sensitivity of l/σ on the reduced EOS is small and it is a same tendency as the LJ potential. Therefore it was found that saturation tendency does not strongly depend on l/σ. Especially, $|dT/d\rho|$ is underestimated relative to the NIST data in the density region above the critical density. In contrast, in the density region below the critical density, the saturation lines agree well with the NIST data. Consequently, we conclude that the effect of molecular orientation on deviation from the principle of corresponding state is small.

On the other hand, in the case of the exp-6 potential, the EOS clearly depends on d and the region of the saturation

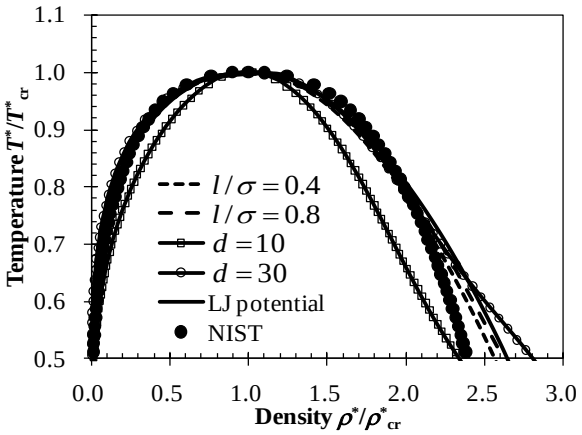

FIGURE 6. COMPARISON OF SIMULATION RESULTS OF TEMPERATURE-DENSITY SATURATION LINE USING EMPIRICAL POTENTIAL AND NIST DATA.

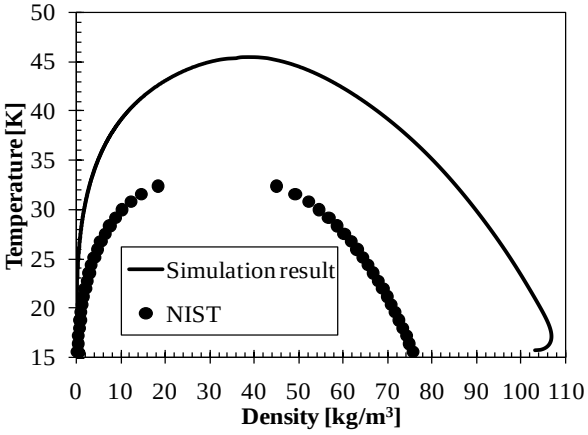

FIGURE 8. COMPARISON OF SIMULATION RESULTS OF TEMPERATURE-DENSITY SATURATION LINE USING *AB INITIO* POTENAIL AND NIST DATA.

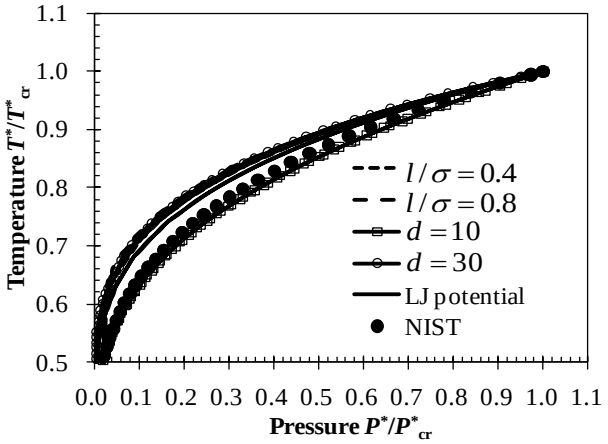

FIGURE 7. COMPARISON OF SIMULATION RESULTS OF TEMPERATURE-PRESSURE SATURATION LINE USING EMPIRICAL POTENTIAL AND NIST DATA.

region is narrow when d is small (d = 10). Therefore, the steepness of the exponential repulsion has a large effect on the estimated thermodynamic properties of hydrogen. However, these empirical potential models are qualitatively consistent with NIST data; *i.e.*, all empirical potentials have the sametendency to underestimate $|dT/d\rho|$ relative to the NIST data for the density region above the critical density. Meanwhile, in the density region below the critical density, empirical potential model could reproduce the thermodynamic properties of cryogenic hydrogen.

These disagreements are considered to be attributed to three effects. The first effect is the quantum effect. The quantum effect influences translational motion, because thermal de Broglie wavelength reaches the length of molecular diameter.

The second effect is the many-body effect. These empirical potential models are simple functions of intermolecular distance using *two-body* forces. Actually, molecular interactions are not described by the sum of pairwise interactions, particularly in higher density region, because the interaction between two molecules is affected by other, surrounding molecules. This is a well-known problem and previous studies say that estimations of saturation properties are improved for higher density regions by considering *three-body* interaction [27, 28]. However, these studies did not consider the quantum effect. Therefore, the effect of *many-body* interaction on quantum systems has not yet been clarified.

The third effect is due to the accuracy of the potential. It is doubtful that these empirical potentials are accurate because these models involve simple functions of intermolecular distance as *two-body* forces and involve only two or three parameters. For this reason, a comparison between the empirical potential and *ab initio* potential was carried out to verify this effect.

The saturation line of the *ab initio* potential is shown in Fig. 8. As shown in Tab. 3 and Fig. 8, the *ab initio* potential overestimates the critical temperature and critical density, based on the NIST data and the absolute values of critical temperature and critical density are not in agreement with each other. We think this disagreement occurs from effect of intermolecular potential model or influence of quantum effect. Next we conducted scaling of *ab initio* potential to clarify the disagreement between simulation results and NIST data.

Scaling was conducted to correspond to the each critical point. That is, $\varepsilon^* = T_{NIST}/T_{ab}$ and $\sigma^* = \rho_{ab}/\rho_{NIST}$ multiplied by each mode potential energy and intermolecular distance of MO calculation results respectively. Where subscript of NIST denote critical points of NIST and subscript of ab denote critical points of *ab initio* potential. The result of scaling the φ^{000} mode potential which has the largest effect on the *ab initio* potential is shown in Fig. 9. As shown in this figure, the displacement between the scaling results and original potential

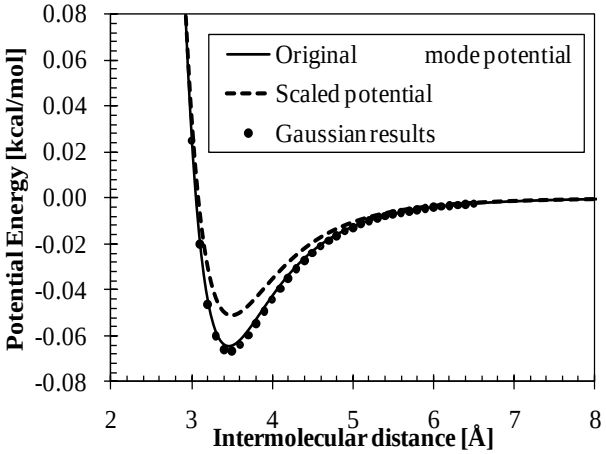

FIGURE 9. COMPARISON BETWEEN ORIGINAL φ^{000} MODE POTENTIAL, SCALED POTENTIAL AND GAUSIAN RESULTS.

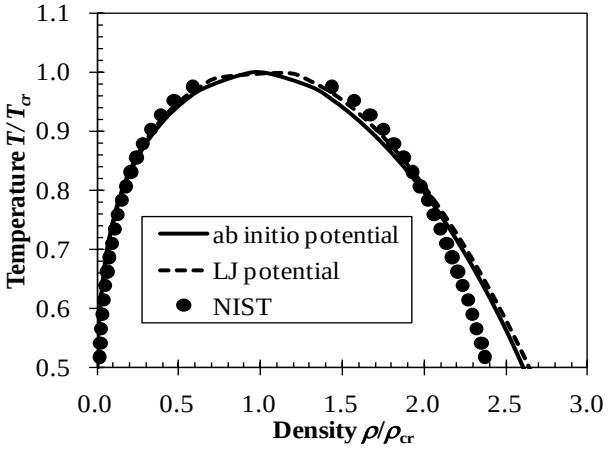

FIGURE 10. COMPARISON BETWEEN SIMULATION RESULTS OF AB INITIO POTENTIAL, LJ POTENTIAL AND NIST DATA USING THE PRINCIPLE OF CORRESPONDING STATES.

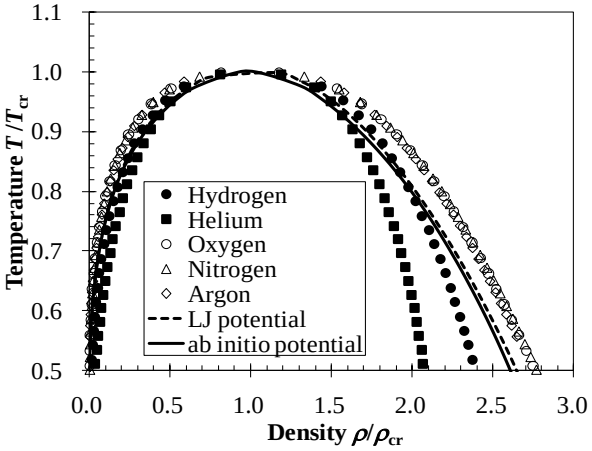

FIGURE 11. COMPARISON OF TEMPERATURE-DENSITY SATURATION LINES OF SIMULATION RESULTS AND EACH FLUID.

is approximately 0.014 kcal/mol at the potential well. It is approximately 0.004 kcal/mol at 6 Å and decreases very gradually beyond 6 Å. Generally speaking, intermolecular interaction energy is very small compared to total energy and is only a few kcal/mol. For example, hydrogen atom has a total energy of 313 kcal/mol including the nuclear energy, electron energy, and electrostatic interaction. On the other hand, the intermolecular interaction energy is only a few kcal/mol. At present, the accuracy of quantum chemical calculation is not more than approximately 2 or 3 kcal/mol, therefore it is very difficult to exactly calculate this difference (0.014 kcal/mol). For this reason, this difference is included in the calculation error. The small difference of intermolecular interaction energy has a large effect on thermodynamic properties of hydrogen. And thus, we consider that the disagreement between the EOS from using the *ab initio* potential and the NIST data is due to errors of the quantum chemical calculation. However, some studies claim that an *ab initio* potential which has the same accuracy as that used in this study can reproduce the second virial coefficient of cryogenic hydrogen by quantum simulations [29-30]. Therefore, it is possible that the reason of the disagreement here is the calculation method.

Next, the effect of *ab initio* potential on the principle of corresponding states was verified to clarify the reason of disagreement between EOS with *ab initio* potential and NIST data. The reduced saturation line is shown in Fig. 10. In this figure the saturation line is reduced by critical temperature T_{cr}, and critical density ρ_{cr} shown in Tab. 3. As shown in Fig. 10, the EOS agrees well with the NIST data in the density region below the critical density and the classical method is able to reproduce the thermodynamic properties. On the other hand, the EOS does not have a qualitatively agreement with the NIST data, and $|dT/d\rho|$ is estimated smaller than the NIST data in the density region above the critical density. This result has the same tendency as those of the empirical potentials. From these results, it is clear that the effect of intermolecular potential model on the estimated thermodynamic properties of cryogenic hydrogen is large, even though the effect of the intermolecular potential model on the displacement in the principle of corresponding states is small.

The reduced saturation lines of helium, hydrogen, oxygen, nitrogen, and argon in the NIST data are shown in Fig. 11 to clarify the reason for the displacement from the principle of corresponding states, where each saturation line is reduced by the critical point. As shown in Fig. 11, the saturation lines of oxygen, nitrogen, and argon, which have a weaker quantum effect, are consistent with each other. On the other hand, the saturation lines of helium and hydrogen which have a stronger quantum effect are not consistent with those of the other fluids, and the widths of their saturation regions are narrower. This

means that the larger the influence of the quantum effect is, the smaller the density at the same temperature and pressure is. This is caused by the influence of increasing the length of the thermal de Broglie wavelength. Molecules which have smaller masses seem to be larger at lower temperature by the quantum effect and therefore the range of their repulsion is also larger. For this reason, pressure is larger and, for the same pressure, the densities are smaller. These same results were reported in previous studies [1, 2]. Moreover, in the case of concerning the quantum effect of cryogenic hydrogen, it is needed to consider the energetically difference between ortho-hydrogen and para-hydrogen. This difference has large effect on the specific heat, however, the effect of this difference on the pressure, temperature and density is small. Therefore, the effect of this energetically difference of hydrogen on this study is small. In summary, we have clarified that even if the scaling potential is used with the classical method, the thermodynamic properties could not be reproduced in the density region above the critical density. We consider the cause is the quantum effect.

COMPARSION OF TRANSPORT COEFFICIENTS

The time history of normalized time correlation function is shown in Fig. 12. Comparison of self-diffusion coefficient of cryogenic hydrogen results and experimental value is presented in Tab. 4. As shown in Fig. 12, time correlation function of transport coefficient converges to 0. This figure shows that correlation of velocity gradually disappears and this behavior is good agreement with typical characteristic of time correlation function [31]. However, calculation results of self-diffusion coefficient using LJ potential is not consistent with experimental value of liquid hydrogen [32]. Even the self-diffusion coefficient which is the simplest transport property because it is calculated using only information of molecular

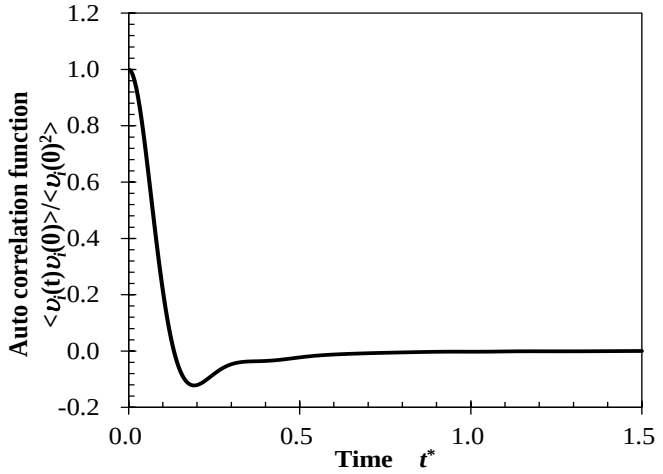

FIGURE 12. NORMALIZED TIME CORRELATION FUNCTION OF SELF-DIFFUSION COEFFICIENT USING LJ POTENIAL MODEL AT $T^*/T_{cr}^* = 0.6079$, $\rho^*/\rho_{cr}^* = 2.640$.

TABLE. 4 THE RESULTS OF EACH TRANSPORT COEFFICIENT USING LJ POTENTIAL AT TRIPLE POINT

	D_s [10^{-9}m^{2}s^{-1}]
This work	4.261
Exp. [32]	19.38

velocity cannot be reproduced using classical molecular dynamics method. We consider this disagreement is arisen from the quantum effect in actual hydrogen molecules which is the influence of increasing the length of the thermal de Broglie wavelength. From this influence, the molecular position and intermolecular force are not simply expressed by classical way. Obviously, velocity of molecule and potential energy are affected by quantum effect. From this result and reason, self-diffusion coefficient of cryogenic hydrogen is not reproduced using classical molecular dynamics method.

CONCLUSION

In this paper, we estimated the thermodynamic properties and transport properties of cryogenic hydrogen using three empirical potential models and *ab initio* potential and clarified the limits of the classical simulation method. Firs, we performed the simulation for a broad range of temperature-density and obtained the EOS, saturation line, and critical point using Kataoka's method for each potential model. We found that the saturation line of hydrogen varies with the tiny displacement of the potential well. Therefore the effect of intermolecular potential model on the estimated thermodynamic properties is large. Moreover, saturation lines reduced by the critical point agree well with NIST data in the density region below the critical density. On the other hand, none of the potential models were consistent with the NIST data in the density region above the critical density and have the same tendency to underestimate $|dT/d\rho|$ relative to the NIST data. The effect of molecular orientation on displacement in the principle of corresponding states is small in the density region above the critical density. In addition, it was clarified by comparison of saturation lines of additional liquids that saturation lines of liquids in which the quantum effect is small agree well with each other, and those in which the quantum effect at low temperatures is large show deviations from other liquids and the widths of their saturation regions were narrower. Consequently, this result suggests that quantum effect is a probable cause of deviations from the principle of corresponding states. Additionally, self-diffusion coefficient was not reproduced using classical method. Besides, the intermolecular potential models which used in this study can express correct pairwise interaction. Therefore, changing the pairwise potential function is insignificant. Moreover, some studies in which thermodynamic properties of cryogenic hydrogen are calculated using non-classical method with similar

pairwise potential model [22] show good agreement with experimental results. These results show that the influence of *many body* interaction [27,28] is smaller than the influence of quantum effect and it is necessary to consider influence of quantum effect not changing the intermolecular potential model. In other words, the thermodynamic properties and transport properties of cryogenic hydrogen in the high density region above the critical density could not be reproduced by classical method.

ACKNOWLEDGEMENT

This study has been supported by the Ministry of Education, Science, Sports and Culture, Grant-in-Aid for Scientific Research (B) (No.19360092) and the Collaborative Research Project of the Institute of Fluid Science, Tohoku University.

REFERENCE

[1] Y. Yonetani and K. Kinugawa, "*Transport properties of liquid para-hydrogen*: *The path integral centroid molecular dynamics approach*", J. Chem. Phys. 119 (2003), pp. 9651-9660.

[2] Y. Yonetani and K. Kinugawa, "*Centroid molecular dynamics approach to the transport properties of liquid para-hydrogen over the wide temperature range*", J. Chem. Phys. 120 (2004), pp. 10624-10633.

[3] A. Nakayama and N. Makri, "*Forward-backward semiclassical dynamics for quantum fluids using pair propagators*: *Application to liquid para-hydrogen*", J. Chem. Phys. 119 (2003), pp. 8592-8605.

[4] D. R. Reichman and E. Rabani, "*A self-consistent mode-coupling theory for dynamical correlations in quantum liquids*: *Application to liquid para-hydrogen*". J. Chem. Phys. 116 (2002), pp. 6279-6285.

[5] J. Cao and G. A. Voth, "*The formulation of quantum statistical mechanics based on the Feynman path centroid density*. I. *Equilibrium properties*", J. Chem. Phys. 100 (1994), pp. 5093-5105.

[6] J. Cao and G. A. Voth, "*The formulation of quantum statistical mechanics based on the Feynman path centroid density*. II. *Dynamical properties*", J. Chem. Phys. 100 (1994), pp. 5106-5117.

[7] J. Cao and G. A. Voth, "*The formulation of quantum statistical mechanics based on the Feynman path centroid density*. III. *Phase space formalism and analysis of centroid molecular dynamics*", J. Chem. Phys. 101 (1994), pp. 6157-6167.

[8] J. Cao and G. A. Voth, "*The formulation of quantum statistical mechanics based on the Feynman path centroid density*. IV. *Algorithms for centroid molecular dynamics*", J. Chem. Phys. 101 (1994), pp. 6168-6183.

[9] J. Cao and G. A. Voth, "*The formulation of quantum statistical mechanics based on the Feynman path centroid density*. V. *Quantum instantaneous normal mode theory of liquid*", J. Chem. Phys. 101 (1994), pp. 6184-6192.

[10] D. R. Reichman, P. N. Rpy, S. Jamg, and G. A. Voth, "*A Feynman path centroid dynamics approach for the computation of time correlation functions involving nonlinear operators*", J. Phys. Chem. 113 (2000), pp. 919-929.

[11] W. H. Miller, "*The Semiclassical Initial Value Representation: A Potentially Practical Way for Adding Quantum Effects to Classical Molecular Dynamics Simulation*", J. Phys. Chem. A. 105 (2001), pp. 2942-2955.

[12] V. A. Zenevich and G. D. Billing, "*Vibrational- rotational energy transfer in H_2 - H_2 collisions.* I. *Semiclassical decoupling approximation*", J. Chem. Phys. 111 (1999), pp. 2401-2406.

[13] K Thompson and N. Makri, "*Influece functional with semiclassical propagators in combined forward-backward time*", J. Chem. Phys. 110 (1999), pp. 1343-1353.

[14] K Thompson and N. Makri, "*Rigorous forward-backward semiclassical formulation of many-body dynamics*", J. Phys. E. 59(1999), pp. R4729-R4732.

[15] E. Rabani and D. R. Reichman, "*A self-consistent mode-coupling theory for dynamical correlations in quantum liquids*: *Rigorous formulation*", J. Chem. Phys. 116 (2002), pp. 6271-6278.

[16] E. Rabani, D. R. Reichman, G. Krilov, and B. J. Berne, "*The calculation of transport properties in quantum liquids using the maximum entropy numerical analytic continuation method*: *Application to liquid para-hydrogen*", Proc. Natl. Acad. Sci. USA. 99 (2002), pp. 1129-1133.

[17] K. Singer, A. Taylor, and J. V. L. Singer, "*Thermodynamic and structural properties of liquids modeled by* '2-*Lennard-Jones centers*' *pair potential*", Mole. Phys. 33 (1977), pp. 1757-1795.

[18] Y. Kataoka,"*Equation of State of the Fluid Defined by the Modified Buckingham (exp-6) Potential Derived by Molecular Dynamics Simulations*"**.** Bull. Chem. Jpn. 65 (1992), pp. 2093-2103.

[19] M. Koshi, K. Shimizu, and S. Tsuda, *Estimation of thermodynamic properties of hydrogen, oxygen and their mixtures based on inter-molecular interactions for rocket engine combustion flow analysis,* Asian Joint Conference on Propulsion and Power 2010, AJCPP2010-153.

[20] Y. Kataoka, "*Studies of liquid water by computer simulations. V. Equation of state of fluid water with Caravetta-Clementi potential*", J. Chem. Phys. 87 (1987), pp. 589-598.

[21] M. P. Allen and D. J. Tildesley, "*Computer Simulation of Liquid*", Clarendon, Oxford. (1986).

[22] I. P. Omelyan, "*On the numerical integration of motion for rigid polyatomic*: *The modified quaternion approach*", Comp. In. Phys. 12 (1998), pp. 97-103.

[23] N. S. Martys and R. D. Mountain, "*Velocity Verlet algorithm for dissipative-particle-dynamics-based models of suspensions*", Phys. Rev. E. 59 (1999), pp. 3733-3736.
[24] T. Kinjo and M. Matsumoto, "*Cavitation processes and negative pressure*", Fluid Phase Equilibria. 144 (1998), pp. 343-350.
[25] E. A. Guggenheim, "*The Principle of Corresponding States*", J. Chem. Phys. 13 (1945), pp. 253-261.
[26] National Institute of Standards and Technology, Chemistry WebBook, http://webbook.nist.gov/chemistry/
[27] B. M. Axilrod and E. Teller, *Interaction of the van der Waals Type Between Three Atoms*". J. Chem. Phys. 11 (1943), pp. 299-300.
[28] J. A. Anta, E. Lomba, and M. Lombardero, "*Influence of three-body forces on the gas-liquid coexistence of simple fluids: The phase equilibrium of argon*", Phys. Rev. E. 55 (1997), pp. 2707-2712.
[29] P. Diep and J. K. Johnson, "*An accurate H_2-H_2 interaction potential from first principles*", J. Chem. Phys. 112 (2000), pp. 4465-4473.
[30] K. Patkowski, W. Chencek, P. Jankowski, K. Szalewicz, J. B. Mehl, G. Garberoglio, A. H. Harvey , "*Potential energy surface for interactions between teo hydrogen molecules*", J. Chem. Phys., 129 (2008), pp. 094304-1-094304-19.
[31] K. Meier, A. Laesecke and S. Kabelac, "*Transport coefficients of the Lennard-Jones model fluid.* II. *Self-diffusion*", J. Chem. Phys., 121 (2004), pp 9526-36849535.
[32] D. E. O'Reilly and E. M. Peterson, "*Self-diffusion of liquid and deuterium*", J. Chem. Phys. 66 (1977), pp. 934-937.